

SAR Image Registration and Segmentation Using an Estimated DEM

C.A. Glasbey

Biomathematics and Statistics Scotland
JCMB, King's Buildings, Edinburgh EH9 3JZ, Scotland

Abstract. Synthetic aperture radar (SAR) images are notoriously difficult to interpret. Segmentation is simplified if a digital map is available, to which the image can be registered. Also, registration is simplified if a digital elevation model (DEM) is available. In this paper it is shown that, if a DEM is unavailable, it can be estimated by minimising an energy functional consisting of a measure of agreement between the SAR image and a digital map together with a thin-plate bending-energy term. A computationally-efficient, finite-element algorithm is proposed to solve the optimisation problem. The method is applied to automatically align an airborne SAR image with a digital map of field boundaries, producing an image which is simultaneously registered and segmented.

1 Introduction

Synthetic aperture radar (SAR) is an active remote-sensing system: microwave radiation is beamed down to the earth's surface from a plane or satellite, a sensor detects the reflected signal, and from this an image is constructed. SAR images are notoriously difficult to interpret, even by eye. For example, Fig 1 shows a log-transformed SAR image of an area near Feltwell, England. A pattern of fields can be discerned, and there is a waterway in the top-right of the image. The small, bright features in the top-right, bottom-left and bottom-right of the image are the result of farm buildings acting as *corner reflectors* to the radar. Many ambiguities remain in the image, such as the positions of some field boundaries.

Pixel values in SAR images are highly variable, a phenomenon termed *speckle*, which makes it desirable to segment the images into homogeneous regions as a first step in their interpretation. Segmentation is often performed manually, an approach which is both tedious and subjective. Glasbey and Horgan [17] used Fig 1 to explore several generic methods for automatic image segmentation, including iterated conditioned modes (ICM) classification [4], thresholding combined with post-classification smoothing by majority filter [30] and Horowitz and Pavlidis's [22] split-and-merge algorithm. These methods were able to distinguish between light and dark fields, but did little more. For other attempts to segment SAR images, see [1, 28], and see [13] for criteria for success.

Domain-specific knowledge, such as constraining boundaries to be straight, and techniques such as the Hough transform [27] and the fitting of snakes [25], could be used to improve the segmentation. However, SAR images are not usually analysed in isolation: a more specific form of domain knowledge is often

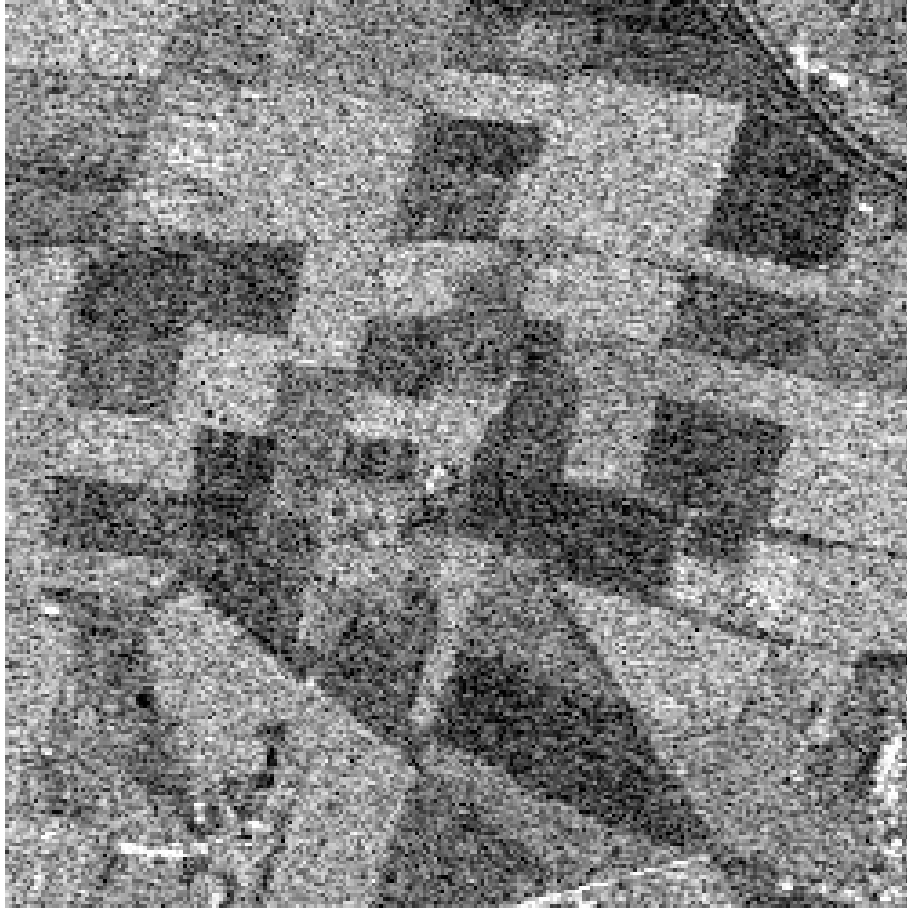


Fig. 1. Log-transformed C-band, HH-polarization, SAR image, obtained by plane in August 1989 during Maestro-1 campaign (Joint Research Centre, Ispra, report IRSA/MWT/4.90).

available in the form of either a digital map or other remotely sensed images. For example, Fig 2 shows a line drawing of field, road and other boundaries for a region approximately corresponding to, but slightly larger than, that imaged by the SAR sensor. By registering the SAR image with this digital map, as a by-product the image is automatically segmented.

Registration of SAR images is important in its own right, irrespective of whether or not we also wish to segment the images, because outputs from SAR interpretation cannot be put to practical use unless their geographical locations are known. SAR image registration is often performed manually (for example, see [12, 14, 36, 11]). Li [29] reviewed automatic methods, distinguishing between



Fig. 2. *Digital line drawing of field, road, and other boundaries for approximately the same region as Fig 1, extracted from a map of an area to the north of the village of Feltwell in East Anglia.*

area- and feature-based ones. The former approach typically involves maximising correlations between small windows in two images, whereas in the latter approach contours or distinctive features are matched between images. Caves et al [10] used linear filters, whereas Kher and Mitra [26] used morphological methods, to locate features in SAR images. Li [29] extracted contours from an optical, remotely-sensed image, and then used elastic warping methods to align them with a SAR image.

Warping is common to many image analysis problems: it may be needed to remove optical distortions introduced by a camera or viewing perspective, to register an image with a reference grid, or to align two or more images. There is a potential conflict between insisting the distortion is smooth and achieving a good match. This can be resolved by an appropriate choice of energy functional. Smoothness can be ensured by assuming a parametric form for the warp, such as a bilinear transformation, or by insisting that the warp satisfies partial differential equations such as Navier's equilibrium equations for elastic bodies [3]. Dependent on the application, matching might be specified by points to be brought into alignment [6], by local measures of correlation between images, or by the

coincidence of edges [9].

Digital elevation models (DEMs), when available, greatly simplify SAR image registration, because the warping can be constrained to be a projective transformation of the DEM [16, 21, 24, 34]. In this paper we show that, if a DEM is unavailable, it can be estimated by minimising an energy functional. This approach is distinct from previous attempts to estimate DEMs using either stereo SAR [15, 33] or interferometric SAR [31]. In § 2, we assume that the ground being imaged is planar, and apply an affine transformation to register the SAR image to the digital map. Then, in § 3 we generalise this approach, by estimating a DEM using a thin-plate spline, to improve the registration. Finally, in § 4 the approach is critically discussed and areas of further work are identified.

2 Affine Transformation

We seek a transformation which maps a position (u, v) on the digital map, where u denotes row number and v denotes column number, to (x, y) in the SAR image. The appropriate transformation is a *projection*. This simplifies to an affine transformation if the ground being imaged can be assumed to be planar and the viewing position is sufficiently distant that foreshortening effects can be ignored. Mathematically, based on Euler's angles [23], we have:

$$\begin{aligned}x &= \alpha + u\gamma \cos \theta + v\gamma \sin \phi \sin \theta \\y &= \beta + u\gamma \sin \theta \sin \psi + v\gamma(\cos \phi \cos \psi - \sin \phi \cos \theta \sin \psi),\end{aligned}$$

involving six unknown parameters $(\alpha, \beta, \gamma, \phi, \theta, \psi)$. This is the most general linear transformation, permitting translation, rotation, different stretching along rows and columns, and shearing. One characterisation is that there is an orthogonal pair of directions in the u - v image which are also orthogonal in the x - y image, and the transformation either stretches or shrinks in these two directions [5]. The inverse transformation $(u, v) \leftarrow (x, y)$ has the same functional form. Therefore, the transformation is guaranteed to be bijective, i.e. it is impossible for folding to occur where two points in the u - v image map to the same point in the x - y image. The affine transformation can be generalised by using a perspective transformation, or by including higher-order polynomials of u and v . See [7, 8, 35] for reviews of geometric transformations.

In order to choose the parameters in the transformation, a measure of agreement between the SAR image and the digital map is required [29]. As a first step, we applied an edge filter to the SAR image. Because of the low signal-to-noise ratio it was desirable to use a large window for the filter. Most edges appear to be step edges, therefore a template matching approach was taken, with the filter output defined to be

$$g_{x,y} = \max_{0 \leq \omega < \pi} \left| \sum_{(x',y') \in S_\omega} f_{x+x',y+y'} - \sum_{(x',y') \in S_{\omega+\pi}} f_{x+x',y+y'} \right| ,$$

for $x, y = 1 \dots n$. Here $f_{x,y}$ denotes the log-transformed SAR value at (x, y) , and S_ω is a semi-circular set of pixel locations specified by

$$S_\omega = \{(x, y) : 0 < x^2 + y^2 \leq r^2, \omega \leq \tan^{-1} y/x < \omega + \pi \pmod{2\pi}\},$$

with \tan^{-1} assumed to produce output over the range 0 to 2π (using, for example, the function **ATAN2** in Fortran77). Fig 3 illustrates the filter, showing pixels with positive and negative weights, for a window of radius $r = 4.5$ pixels and a particular choice of ω . This size of window appeared to be most effective in locating edges in the SAR image. For efficient computation, at each (x, y) -location, output can be computed recursively as ω is increased. Fig 4 shows the result of applying the edge filter to Fig 1. Output has been scaled so the largest values appear black and zero values appear white.

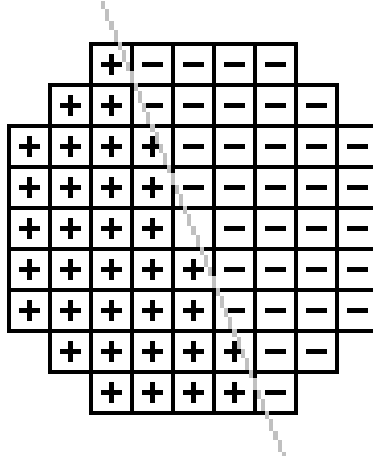


Fig. 3. An illustration of the edge filter: pixels with positive and negative weights are shown, for a window of radius $r = 4.5$ pixels, and a particular choice of ω corresponding to an edge shown by the grey line.

The measure of agreement between Fig 4 and a warped version of Fig 2 was defined by the energy functional:

$$E = \frac{1}{N_S} \sum_{(u,v) \in S} (\tilde{g} - g_{x,y}) ,$$

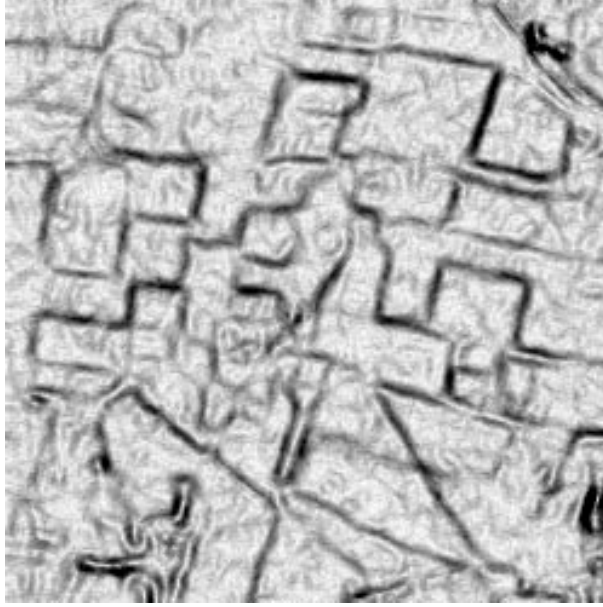


Fig. 4. Result of applying edge filter to Fig 1.

where $S = \{(u, v) : M_{u,v} = 1, 1 \leq x, y \leq n\}$ is the set of all black points in the digital map (indicated by $M_{u,v} = 1$) which transform to points (x, y) within the region of Fig 4, N_S denotes the number of points in S (which will depend on the parameters in the affine transformation) and \bar{g} is the mean pixel value in Fig 4. Thus, the energy functional is an inner product between Figs 2 and 4, after mean correction.

The matching problem becomes one of finding the values of the affine parameters which minimise E . Unfortunately, the function to be minimised has many local minima. Therefore, it is necessary to conduct a grid search to determine good starting values for the parameters, before using an iterative optimisation algorithm to locate the minimum. We proceeded in two stages:

1. Initially we limited ourselves to a four-parameter family of rectangular transformations, by setting $\phi = \psi = 0$. E was evaluated for a range of values of the parameters, and the best value was used as a starting value for the Nelder-Mead simplex algorithm, implemented as NAG routine E04CCF [32].
2. We then considered the six-parameter affine transformation, starting the Nelder-Mead algorithm from the best fitting rectangular transformation.

Fig 5 shows the final result: the outline of the map boundaries is displayed rather than the boundaries themselves, in order to show the alignment more clearly. Agreement appears to be close between the edges in the SAR image and the map, except that a few field boundaries are absent from the map. Detailed examination

also reveals some places where the boundaries are slightly displaced, for example at the bottom-centre and bottom-right of Fig 5, suggesting that the assumption of level ground is not quite appropriate. Therefore, in § 3 we generalise the approach to include estimation of a DEM in the registration procedure.



Fig. 5. *Map aligned with edge-filtered SAR image using an affine transformation (the outline of the map boundaries is displayed rather than the boundaries themselves).*

3 Thin-plate Spline DEM

Parametric transformations do not perform well in the presence of local distortions. Splines offer one alternative, either piecewise linear [18] or cubic [19]. Equating warping with the distortions achievable on an elastic sheet is one way of introducing smoothness constraints. Bajcsy and Kovacic [3] invoked Navier's equilibrium equations for elastic bodies, which they insisted on being satisfied at all points except those where a match between images had been identified. Solution requires the use of finite element methods. Burr [9] used sums of Gaussian weight functions to interpolate between matched points, justifying them as an elastic Green's function in an appropriate medium. Tang and Suen [35] found transformations which minimised a harmonic function. Again finite element methods are required. Note that Kass et al [25] used similar methods to constrain *snakes* to be smooth.

Another approach is to regard a warping as two two-dimensional surfaces, corresponding to x as a function of u and v , and similarly y as a function of u and v . Arad et al [2] used a sum of radial basis functions plus affine transforms to represent the x -transformation:

$$x = \sum_{i=1}^m \eta_i F \left(\sqrt{(u - u_i)^2 + (v - v_i)^2} \right) + \xi_0 + \xi_1 u + \xi_2 v,$$

where $(u_1, v_1) \dots (u_m, v_m)$ are a set of m labelled points and F is a radial basis function, and similarly for the y -transformation. Many choices of F correspond to the minimisation of some energy functional. In particular, the thin-plate spline, $F(z) = z^2 \log z$, leads to a surface which minimises

$$\sum_{i=1}^m \{x_i - x(u_i, v_i)\}^2 + \lambda J(x),$$

with respect to the function x , where the m labelled points are warped to x -coordinates $x_1 \dots x_m$,

$$J(x) = \int \int_{-\infty}^{\infty} \left\{ \left(\frac{\partial^2 x}{\partial u^2} \right)^2 + 2 \left(\frac{\partial^2 x}{\partial u \partial v} \right)^2 + \left(\frac{\partial^2 x}{\partial v^2} \right)^2 \right\} du dv$$

denotes the bending energy of a thin plate and λ is a non-negative constant which controls the smoothness of the warping. Larger values of λ produce smoother results, but with poorer alignment of the labelled points. Coefficients $\eta_1 \dots \eta_m, \xi_0, \xi_1$ and ξ_2 can be obtained as the solution of $(m + 3)$ simultaneous linear equations [20].

Pairs of thin-plate splines have no physical interpretation in the context of image warping; their use is entirely ad hoc. However, in applications such as ours, which consists of a projective view of a surface, a single thin-plate spline can be used with physical motivation, although it will not permit any step changes in elevation. We assume that the elevation $h_{u,v}$ at map location (u, v) is specified by a thin-plate spline. The energy functional from § 2 is generalised to include a bending energy term:

$$E = \frac{1}{N_S} \sum_{(u,v) \in S} (\bar{g} - g_{x,y}) + \lambda J(h),$$

and the projective transformation [23] generalises the affine transformation:

$$\begin{aligned} x &= \alpha + u\gamma \cos \theta + v\gamma \sin \phi \sin \theta + h_{u,v} \gamma \cos \phi \sin \theta \\ y &= \beta + u\gamma \sin \theta \sin \psi + v\gamma (\cos \phi \cos \psi - \sin \phi \cos \theta \sin \psi) \\ &\quad - h_{u,v} \gamma (\sin \phi \cos \psi + \cos \phi \cos \theta \sin \psi). \end{aligned}$$

This problem lacks an analytic solution, but can be solved numerically using finite element methods. We divide the map into a $(p + 1)$ by $(p + 1)$ grid, and specify the elevations of the $(p + 1)^2$ points

$$(k\Delta_u, l\Delta_v) \quad \text{for } k, l = 0, \dots, p,$$

by $H_{k,l}$, where $\Delta_u = n_u/p$, $\Delta_v = n_v/m$ and the digital map is $n_u \times n_v$ pixels in size. Then we use bilinear interpolation for the elevation of intermediate points. If

$$k\Delta_u \leq u \leq (k+1)\Delta_u \quad \text{and} \quad l\Delta_v \leq v \leq (l+1)\Delta_v,$$

then

$$\begin{aligned} h_{u,v} = & H_{k,l} + (H_{k+1,l} - H_{k,l}) \left(\frac{u}{\Delta_u} - k \right) + (H_{k,l+1} - H_{k,l}) \left(\frac{v}{\Delta_v} - l \right) \\ & + (H_{k+1,l+1} - H_{k+1,l} - H_{k,l+1} + H_{k,l}) \left(\frac{u}{\Delta_u} - k \right) \left(\frac{v}{\Delta_v} - l \right). \end{aligned}$$

It follows from the projective transformation that x and y are also piecewise bilinear. $J(h)$ can be approximated, to within a scaling term, by

$$\begin{aligned} & \sum_{k=1}^{p-1} \sum_{l=0}^p \left(\frac{H_{k+1,l} + H_{k-1,l} - 2H_{k,l}}{\Delta_u^2} \right)^2 \\ & + 2 \sum_{k=0}^{p-1} \sum_{l=0}^{p-1} \left(\frac{H_{k+1,l+1} + H_{k,l} - H_{k,l+1} - H_{k+1,l}}{\Delta_u \Delta_v} \right)^2 \\ & + \sum_{k=0}^p \sum_{l=1}^{p-1} \left(\frac{H_{k,l+1} + H_{k,l-1} - 2H_{k,l}}{\Delta_v^2} \right)^2. \end{aligned}$$

The parameters $H_{k,l}$ can be estimated to minimise the energy functional. This was done by perturbing each elevation in turn to minimise E , while keeping the projective transform parameters fixed at the values estimated in § 2. Note that the speed of computation can be improved significantly by only computing local terms in E after each adjustment in $H_{k,l}$, and at each iteration only perturbing elevations one of whose neighbours was changed at the previous iteration. The optimisation was started with $H_{k,l}$ set to zero in a 17×17 grid and $\lambda = 1000$, a value established by trial-and-error to allow sufficient changes in elevation to align the image with the map, but without producing a very rough DEM. The elevations estimated by the algorithm are shown in perspective in Fig 6.

Fig 7 shows an outline of the map boundaries aligned with the edge-filtered SAR image. The result is very similar to Fig 5 but, in particular, note the improved fit at several positions, including the bottom of the map. The average strength of the aligned edges is increased by 40%. However, there is some evidence that the warping is too severe in the top-right of the image, where the waterway has been distorted to align with a bright feature which is probably a building, and as a consequence the waterway does not appear to be horizontal in Fig 6. Fig 8 shows the SAR image registered with the digital map, obtained by inverting the projective transformation. The alignment can be seen to be very good, and automatically yields an almost complete segmentation of the image. It is a relatively straightforward task to identify, and further partition, the few heterogeneous segments.

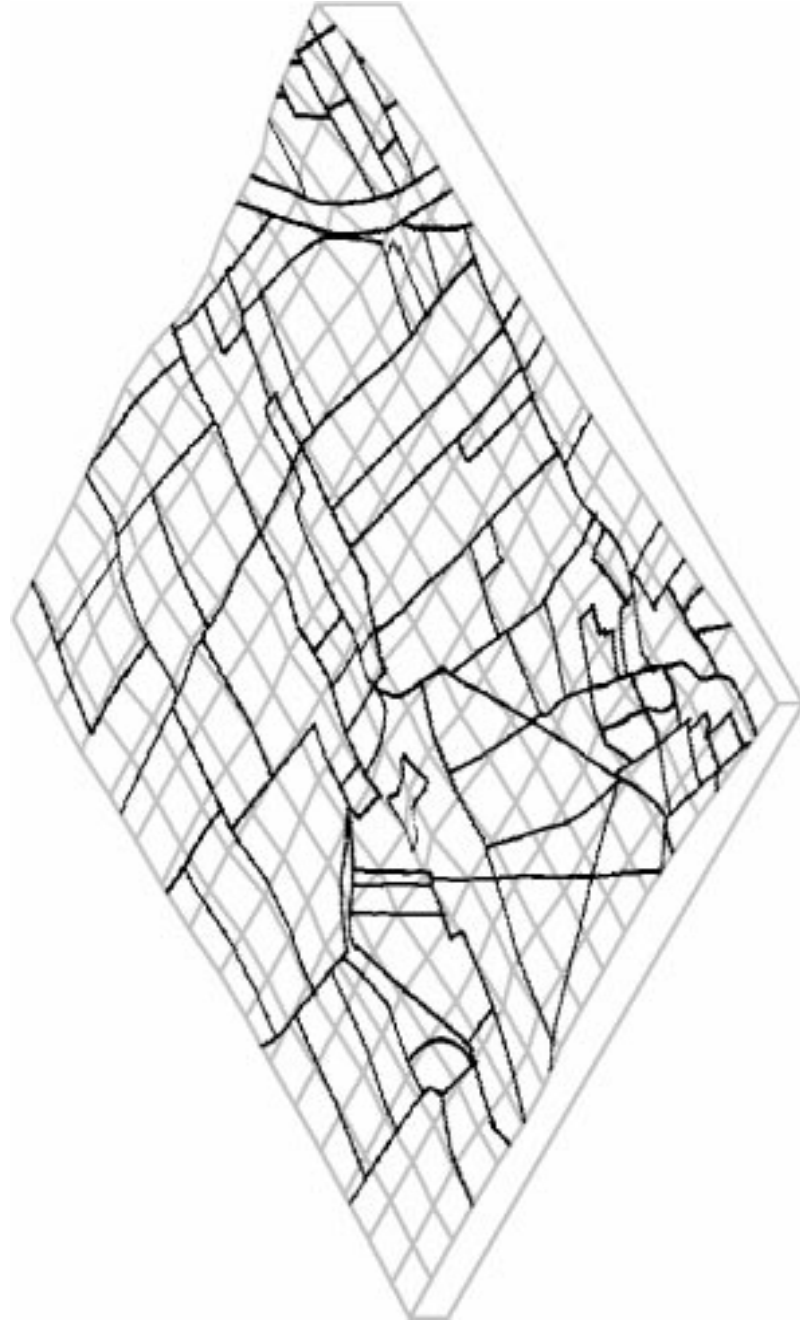


Fig. 6. *Perspective view of map with DEM estimated using a thin-plate spline.*

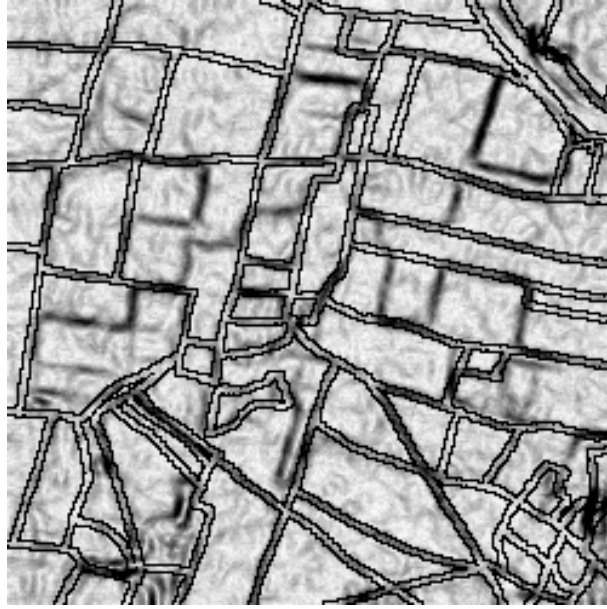


Fig. 7. *Map aligned with edge-filtered SAR image using a thin-plate spline transformation (the outline of the map boundaries is displayed rather than the boundaries themselves).*

4 Discussion

We have shown how SAR images can be automatically registered with digitised maps while yielding, as by-products, segmentations of the images and estimated DEMs. Much work remains to be done, primarily to validate the method by comparing estimated and known DEMs for a range of images. Results also need to be compared with those from other approaches to SAR registration, such as [10, 29]. However, the new method should perform better because of the physically-based constraint on the warping.

The method is open to many refinements, such as the use of other edge filters, development of criteria for choosing the smoothing parameter λ in the energy functional, and improvements to the efficiency and robustness of the optimisation algorithm. For example, the projective transform parameters could be adjusted to take account of the estimated DEM. It would also be of interest to use the method to register SAR and optical, remotely-sensed images.

Acknowledgements

The work was supported by funds from the Scottish Office Agriculture, Environment and Fisheries Department.



Fig. 8. *Superposition of aligned SAR image with map.*

References

1. Ali, S.M., Burge, R.E.: New automatic techniques for smoothing and segmenting SAR images. *Signal Processing* **14** (1988) 335–346
2. Arad, N., Dyn, N., Reisfeld, D., Yeshurun, Y.: Image warping by radial basis functions: applications to facial expressions. *CVGIP: Graphical Models and Image Processing* **56** (1994) 161–172
3. Bajcsy, R., Kovacic, S.: Multiresolution elastic matching. *Computer Vision, Graphics and Image Processing* **46** (1989) 1–21

4. Besag, J.: On the statistical analysis of dirty pictures (with discussion). *Journal of the Royal Statistical Society, Series B* **48** (1986) 259–302
5. Bookstein, F.L.: *The Measurement of Biological Shape and Shape Change*. Springer-Verlag, Berlin (1978)
6. Bookstein, F.L.: Principal Warps: thin plate splines and the decomposition of deformations. *IEEE Transactions on Pattern Analysis and Machine Intelligence* **11** (1989) 567–585
7. Bookstein, F.L.: *Morphometric Tools for Landmark Data : Geometry and Biology*. Cambridge University Press, Cambridge (1991)
8. Brown, L.G.: A survey of image registration techniques. *ACM Computing Surveys* **24** (1992) 325–376
9. Burr, D.J.: A dynamic model for image registration. *Computer Graphics and Image Processing* **15** (1981) 102–112
10. Caves, R.G., Harley, P.J., Quegan, S.: Matching map features to synthetic aperture radar (SAR) images using template matching. *IEEE Transactions on Geoscience and Remote Sensing* **30** (1992) 680–685
11. Cihlar, J., Pultz, T.J., Gray, A.L.: Change detection with synthetic aperture radar. *International Journal of Remote Sensing* **13** (1992) 401–414
12. Collins, M.J., Livingstone, C.E.: On the dimensionality of multiparameter microwave image data from thin sea-ice in the Labrador-sea. *IEEE Transactions on Geoscience and Remote Sensing* **34** (1996) 114–136
13. Delves, L.M., Wilkinson, R., Oliver, C.J., White, R.G.: Comparing the performance of SAR image segmentation algorithms. *International Journal of Remote Sensing* **13** (1992) 2121–2149
14. Dobson, M.C., Pierce, L.E., Ulaby, F.T.: Knowledge-based land-cover classification using ERS-1/JERS-1 SAR composites. *IEEE Transactions on Geoscience and Remote Sensing* **34** (1996) 83–99
15. Fernandes, D., Waller, G., Moreira, J.R.: Registration of SAR images using the chirp scaling algorithm. *IGARSS'96 – International Geoscience and Remote Sensing Symposium* (1996) 799–801
16. Frankot, R.T., Hensley, S., Shafer, S.: Noise resistant estimation techniques for SAR image registration and stereo matching. *IGARSS'94 – International Geoscience and Remote Sensing Symposium* (1994) 1151–1153
17. Glasbey, C.A., Horgan, G.W.: *Image Analysis for the Biological Sciences*. Wiley, Chichester (1995)
18. Goshtasby, A.: Piecewise linear mapping functions for image registration. *Pattern Recognition* **19** (1986) 459–466
19. Goshtasby, A.: Piecewise cubic mapping functions for image registration. *Pattern Recognition* **20** (1987) 525–533
20. Green, P.J., Silverman, B.W.: *Nonparametric Regression and Generalised Linear Models: a roughness penalty approach*. Chapman and Hall, London (1994)
21. Guneriusson, T., Johnsen, H., Sand, K.: DEM corrected ERS-1 SAR data for snow monitoring. *International Journal of Remote Sensing* **17** (1996) 181–195
22. Horowitz, S.L., Pavlidis, T.: Picture segmentation by a tree traversal algorithm. *Journal of the Association for Computing Machinery* **23** (1976) 368–388
23. Ito, K. (ed.): *Encyclopedic Dictionary of Mathematics* (2nd edition). MIT Press, Massachusetts (1987) 1729
24. Johnsen, H., Lauknes, L., Guneriusson, T.: Geocoding of fast-delivery ERS-1 SAR image mode product using DEM data. *International Journal of Remote Sensing* **16** (1995) 1957–1968

25. Kass, M., Witkin, A., Terzopoulos, D.: Snakes: active contour models. *International Journal of Computer Vision* **1** (1988) 321–331
26. Kher, A., Mitra, S.: Registration of noisy SAR imagery using morphological feature extractor and 2-D cepstrum. *Applications of Digital Image Processing XV* (1993) 281–291
27. Leavers, V.F.: *Shape Detection in Computer Vision Using the Hough Transform*. Springer-Verlag, London (1992)
28. Lee, J.S., Jurkevich, I.: Segmentation of SAR images. *IEEE Transactions on Geoscience and Remote Sensing* **27** (1989) 674–680
29. Li, H., Manjunath, B.S., Mitra, S.K.: A contour-based approach to multisensor image registration. *IEEE Transactions on Image Processing* **4** (1995) 320–334
30. Mardia, K.V., Hainsworth, T.J.: A spatial thresholding method for image segmentation. *IEEE Transactions on Pattern Analysis and Machine Intelligence* **10** (1988) 919–927
31. Marechal, N.: Tomographic formulation of interferometric SAR for terrain elevation mapping. *IEEE Transactions on Geoscience and Remote Sensing*, 1995 **33** (1995) 726–739
32. Numerical Algorithms Group: *Library Manual Mark 16*. NAG Central Office, 256 Banbury Road, Oxford OX2 7DE, UK (1993)
33. Prati, C., Rocca, F.: Limits to the resolution of elevation maps from stereo SAR images. *International Journal of Remote Sensing* **11** (1990) 2215–2235
34. Takeuchi, S.: Image registration between SAR and TM data using DEM and slant range information. *IGARSS'93 – International Geoscience and Remote Sensing Symposium* (1993) 1351–1353
35. Tang, Y.Y., Suen, C.Y.: Image transformation approach to nonlinear shape restoration. *IEEE Transactions on Systems, Man and Cybernetics* **23** (1993) 155–172
36. Vornberger, P.L., Bindschadler, R.A.: Multispectral analysis of ice sheets using co-registered SAR and TM imagery. *International Journal of Remote Sensing* **13** (1992) 637–645